Journal of Power Sources 207 (2012) 19–29

Contents lists available at SciVerse ScienceDirect

Journal of Power Sources

journal homepage: www.elsevier.com/locate/jpowsour

Nature of contact corrosion layers on lead alloys: A study by impedance spectroscopy☆

M.M. Burashnikova*, I.A. Kazarinov, I.V. Zotova

Saratov State University named after N.G. Chernishevsky, 83 Astrakhanskaya Str., Saratov 410012, Russian Federation

ARTICLE INFO

Article history:
Received 15 October 2011
Received in revised form
18 December 2011
Accepted 20 December 2011
Available online 30 December 2011

Keywords:
Lead-acid battery
Lead alloys
Corrosion layer
Electrochemical impedance spectroscopy (EIS)

ABSTRACT

Corrosion layers on lead, lead–antimony and lead–calcium alloys doped with various components (Cd, Sn, Ba, and Ag) were studied using impedance spectroscopy. The films were formed under different potentials and polarization conditions in 4.8 M sulfuric acid solution. The nature of the corrosion layer formed at the alloy-oxidation products interphase was studied using impedance spectroscopy. The results show that the processes proceeding at this boundary can be simulated with an equivalent circuit corresponding to a two-layer model of the corrosion film (an outer high-conducting part and an inner low-conducting one). Parameters of the proposed equivalent circuits were estimated.

1. Introduction

Alloy selection for the current collectors of positive electrodes is a topical problem at the designing of valve-regulated lead-acid batteries. Such alloys must have good mechanical and casting properties, low corrosion rates, and a good conductivity of the contact corrosion layer formed at the current collector—active mass interface during the operation. The corrosion layer formed on the current collector surface plays an essential role in the battery functioning. According to the article [1] the low conductivity of the corrosion layer on the current collector/active mass interface may restrict the service life of the battery down to 20–30 cycles. Such a strong influence of the corrosion layer characteristics on the battery performance is determined by the fact that the total current generated by the active mass finally passes through this layer. The properties of the corrosion layer are influenced by the grid alloy composition, active mass composition, the mode, depth and rate of charging and discharging. The structure and composition of corrosion films are complex and depend on many factors. On the basis of X-ray and electrochemical measurements, Pavlov [2] has proposed that the nature of the passive film formed on the lead electrode can be divided on three potential ranges. The passive layer formed within −0.62 to 0.05 V contains $PbSO_4$ crystals. The layer formed from 0.05 to 1.3 V has an external bed composed of $PbSO_4$ and an internal bed comprising the basic lead compounds (mainly PbO and basic lead sulfates) which grows under the primary porous $PbSO_4$ layer. At the potentials more positive than 1.3 V, α and β-PbO_2 become the main anode products. However, there was found [3] that the internal layer of PbO under the previously grown $PbSO_4$ layer on the lead electrode forms under potentials more positive than −0.2 V. The properties of both layers (the external and internal) depend on potential and dwell time.

Pb–Ca (lead–calcium), Pb–Sn (lead–tin), and Pb–Sb (lead–antimony) alloys are widely used as materials for the current grids in production lead-acid batteries [4–7]. The usage of lead–antimony alloys provides a good cyclability of batteries, mainly due to the corrosion film, which is formed on the current collector surface and consists of well-conducting lead dioxide. However, the low hydrogen overpotential on the negative grid is a disadvantage of these alloys. Lower antimony contents in the alloy not only worsen the mechanical and casting characteristics but also significantly increase the corrosion layer resistance. Lower antimony contents in the alloy should be compensated by other components, for example, tin [5,8–10], cadmium [11], and arsenic.

The designing of valve-regulated lead-acid batteries requires the usage of low-antimony or even antimony-free alloys for positive current collectors. Thus lead–tin and lead–calcium alloys can be used [12]. The lead–calcium alloys have higher hydrogen overpotential and, hence, lower rates of water loss in the battery and its self-discharge. However, the usage of such alloys brings to

☆ Presented at the LABAT'2011 Conference, Albena, Bulgaria, 7–10 June 2011.

* Corresponding author. Tel.: +7 8452 516413; fax: +7 8452 271491.
E-mail address: burashnikova_mm@mail.ru (M.M. Burashnikova).

0378-7753/$ – see front matter © 2011 Elsevier B.V. All rights reserved.
doi:10.1016/j.jpowsour.2011.12.042

premature capacity loss, which is associated with the formation of a poorly conducting barrier corrosion layer on the current collector/active mass interface. In order to improve the conductivity of the passive corrosion layer and the cyclability of lead-acid batteries, lead–calcium alloys are doped with such components as tin [13–17], silver [18], and barium [19].

The aim of this research was to study the properties of the corrosion films on lead, lead–calcium and lead–antimony alloys doped with various components (Cd, Sn, Ba, and Ag) by means of impedance spectroscopy.

2. Experimental

2.1. Preparation of working electrodes

Pure Pb 99.99 wt.% and the following lead alloys were prepared for our experiments:

Pb –*x* wt.% Sn (*x* = 1.0, 1.5, 2.0, 3.0); Pb –1.0 wt.% Sn –*x* wt.% Ca –0.015 wt.% Al (*x* = 0.01, 0.06, 0.08); Pb –1.0 wt.% Sn –0.06 wt.% Ca –0.23 wt.% Ag –0.015 wt.% Al; Pb –1.0 wt.% Sn –0.06 wt.% Ca –0.015 wt.% Ba –0.015 wt.% Al; Pb –4.9 wt.% Sb –0.2 wt.% Sn; Pb –1.9 wt.% Sb –0.2 wt.% Sn; Pb –1.5 wt.% Sb –1.5 wt.% Cd.

The Pb–Sn alloys were prepared by means of direct fusion of the pure components.

The Pb–Sn–Ca–Al alloy was prepared by introduction of a calcium–aluminum alloy into the lead–tin one. Aluminum is used for calcium protection from oxidation. The composition of the Ca–Al alloy corresponded to eutectics (Ca (73 wt.%)–Al (27 wt.%)) [20].

The silver-doped alloy was obtained by introduction of a calcium–aluminum alloy into the lead–tin one and addition of silver (0.023 wt.%).

The barium-containing alloy was prepared by fusion of the lead–tin, calcium–aluminum and lead–barium alloys. The lead–barium alloy had its eutectic composition [Pb (90 wt.%)–Ba (10 wt.%)] [20].

The lead–antimony alloys were prepared by means of direct fusion of their pure components.

The alloy components were fused in alundum crucibles placed into a resistance furnace, at 500 °C (for the calcium–aluminum and lead–barium alloys the temperature was 850 °C) during 3 h in an argon atmosphere. Then they were cast into a fluoroplastic mould which was heated up to 200 °C. The obtained round plates of a 25 mm diameter and a 2 mm thickness were kept in the furnace at 200 °C during 5 h for ageing. A sample was prepared from each alloy and then welded to a lead wire to be used as a working electrode for electrochemical measurements. A part of the electrode with the place of seal was covered with an insulating varnish (CAPON) to avoid any contact with the electrolyte.

A surface of the working-electrode was prepared by mechanical polishing with emery paper with successive decreasing the grain size down to 10 μm. Then, it was polished with thick felt and immersed into a special solution for chemical polishing of lead (99 vol.% CH_3COOH, 1 vol.% H_2O_2). The working electrode was washed with double-distilled water and ethanol before immersing into the electrolyte solution.

2.2. Cyclic voltammetry (CV) and electrochemical impedance spectroscopy (EIS) measurements

A three-electrode conventional glass cell was used for electrochemical measurements. An Ag/AgCl/KCl electrode served for the comparison (E_0 = 0.201 V vs. SHE at 25 °C). A platinum plate (Pt 99.99%) was used as an auxiliary electrode. The electrolyte, a 4.8 M H_2SO_4 solution, was prepared from H_2SO_4 and double-distilled water. Before each experiment, a cathode potential of −1.0 V was applied for 10 min in order to reduce any oxides formed during pretreatment. All potentials reported here are referenced to the standard hydrogen electrode (vs. SHE).

Cyclic voltammetry (CV) and electrochemical impedance spectroscopy (EIS) measurements were performed using an AUTOLAB PGSTAT302N controlled by a personal computer. Cyclic voltammetric curves were recorded in two ways for each electrode, namely, (a) at a potential scanning rate 1 mV s^{-1} during five cycles within a potential range from −0.9 to 2.5 V; (b and c) at a potential scanning rate 20 mV s^{-1} during hundred cycles within potential ranges from −0.9 to 0.0 and from 1.5 to 2.5 V.

A corrosion film was formed on the studied electrodes before the impedance measurements. The corrosion film on the lead electrode surface was formed under several potentials during one hour after preliminary cycling (5 cycles) from −1.0 V to the potential of film formation. Then, an impedance spectrum was recorded at the same potential. Impedance was measured just after the corrosion layer growth in the same cell and at the same potential within a frequency range from 100 kHz to 1 mHz with amplitude 10 mV. All measurements were made at room temperature. The recorded impedance spectra were processed by ZView® 3.0a software (Scribner Associates, Inc.) with selection of equivalent circuits.

2.3. Metallographic examinations

Cylinder samples of a 0.5 cm diameter were made for microstructural analysis of lead alloys. The side surface of each cylinder was insulated with Teflon cover. The end surface of the samples was mechanically ground by emery paper of different quality. Then the samples were carefully washed with distilled water, polished chemically in a solution of the following composition: 1.5 ml of 50% hydrogen peroxide and 48.5 ml of icy acetic acid. After this, the electrode was polished with thick felt and washed with distilled water once again.

The micrographic specimens were etched during 3 h without heating or 0.5–2 min in a heated (up to 70–80 °C) solution of the following composition: 10 ml of concentrated acetic acid; 10 ml of concentrated nitric acid; 40 ml of glycerol. Then they were washed with distilled water. The surface of the samples was examined by means of a metallographic digital Altami MET1M complex equipped with a digital camera and connected to a PC.

2.4. Corrosion test

The corrosion resistance of the alloys under examination was estimated by the weight loss of the samples after their oxidation in potentiostatic conditions and oxide film removal. The samples as disks of a 2.3 cm diameter were kept at a potential of 2.15 V (vs. SHE) in a three-electrode cell in a 4.8 M solution of sulfuric acid at 40 °C. The duration of anodic polarization of the electrodes was 10, 30, 60, and 180 min. Under this anode potential, lead alloys are oxidized to lead dioxide with oxygen release. Therefore, we have selected more severe conditions for corrosion tests of alloys in comparison with those taking place in real LAB, where the positive electrode is under such potentials at significant overcharges only.

Prior to measurements, the electrodes were thoroughly washed with distilled water and treated with ethanol; each electrode was dried and weighed. The oxide film formed was removed during 30 min in a boiling solution of the following composition: 80 g dm^{-3} of sodium hydroxide; 50 g dm^{-3} of mannitol; 0.62 g dm^{-3} of hydrazine sulfate. This solution had been found not to dissolve the metal components of the alloy at boiling. Further, the electrodes were washed with distilled water, dried, and weighed once again.

The corrosion weight loss in mg cm^{-2} was calculated by the following formula:

$$\Delta m = \frac{m_0 - m_1}{S}$$

where m_0 is the initial weight of the sample, mg; m_1 – the weight of the sample on removal of the corrosion products, mg; S – the surface area of the sample before the test, cm^2.

2.5. X-ray analysis

X-ray phase analysis was carried out on a DRON-4 diffractometer with the usage of an X-ray tube with a copper anode (Cu Kα radiation). Diffractograms were analyzed by using the PCPDFWIN database (JCPDS, v. 2.02, 1999).

2.6. Scanning electron microscopy (SEM) imaging

Morphological studies were performed by means of a MIRA 2 LMU scanning electronic microscope equipped with a system of energy-dispersion microanalysis (INCA Energy). The resolution of this microscope reaches 5 nm, and the sensitivity of the INCA Energy detector is 133 eV/10 mm^2, which enables analysis of chemical elements from beryllium to plutonium to be carried out in deep vacuum.

3. Results and discussion

3.1. Characterization of alloy

To study general characteristics of the electrochemical behavior of electrodes made of lead and our alloys in sulfuric acid, cyclic voltammetric curves were recorded.

Fig. 1 presents a cyclic voltammetric curve for the lead electrode within a potential range from hydrogen release to oxygen release (a), and potentiodynamic curves of cycling in both cathode (b) and anode (c) regions, respectively. All potentials are given with respect to SHE.

The recorded curve (Fig. 1a) is characterized by the following processes: a maximun of current (peak 1) is observed at direct run in the cathode range, which corresponds to lead oxidation to lead sulfate. As the anode polarization rises further, a wide range of the passive state is observed just to peak 2, associated with oxygen release onset. At back run, peak 3 of PbO_2 reduction is distinctly seen at E = 1.7 V, this substance having been accumulated in the oxygen release range. Two peaks are noticeable in the cathode part of the cyclic votammogram, they correspond to reduction of PbO (peak 4) and $PbSO_4$ (peak 5), respectively, to lead. When this process is finished, a sharp growth of current is observed due to hydrogen release on the lead elecrtrode. At cycling within from −0.7 to 0 V, only one peak caused by $PbSO_4$ reduction to lead is fixed on the voltammetric curve at back run. At cycling within from 1.5 to 2.5 V, a distinct peak associated with PbO_2 formation is observed at direct run.

Fig. 2 compares typical cyclic potentiodynamic curves for the electrode made of pure lead and lead–tin alloys within potential ranges from −0.7 to 0.0 V (a and c) and from 1.4 to 2.4 V (b and d) at the 1st and 40th cycle, respectively. One can see that when tin makes up 1, 1.5, and 2% in the alloy, the electrochemical activity of the electrodes made of these alloys is reduced in comparison with pure lead. However, when tin in the alloy is increased up to 3%, its electrochemical activity significantly rises just at the 1st cycle in both ranges examined. The peak corresponding to Pb oxidation to $PbSO_4$ for this alloy shifts towards the negative range. Hence, increasing the tin content up to 3% brings to more intense alloy dissolution. A similar trend remains within from 1.4 to 2.4 V as well,

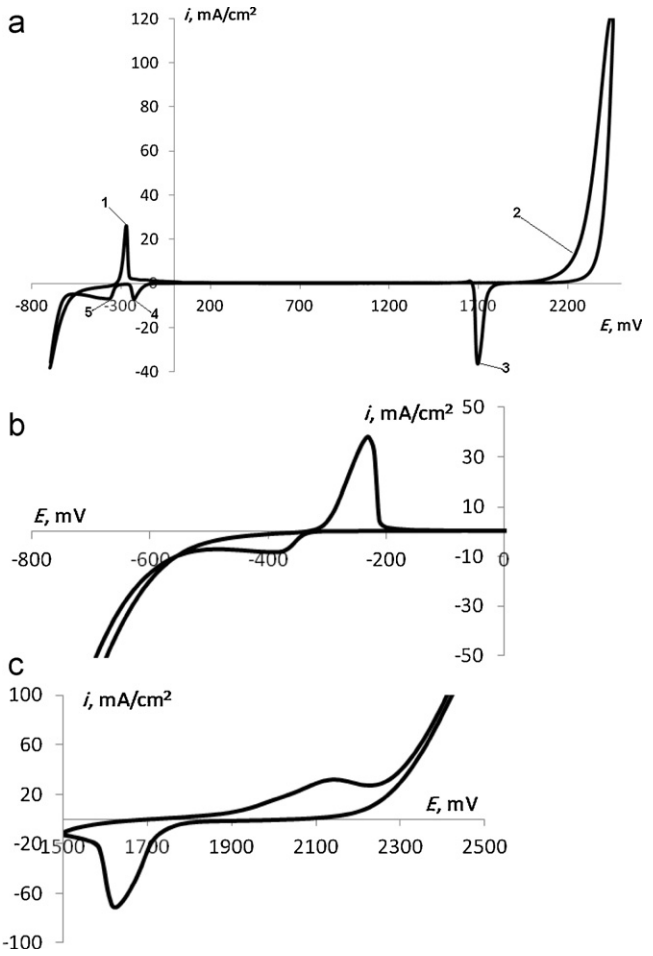

Fig. 1. Cyclic voltammogram for a Pb electrode in potential area from −0.9 V to 2.3 V (vs. SHE). Cycle number – 40; scan rate – 10 mV s^{-1} (a) cyclic voltammograms for a Pb electrode in potential area from −0.7 to 0 V (b) and from 1.5 to 2.5 V (c) (vs. SHE). Cycle number – 100; scan rate – 20 mV s^{-1}.

where $PbSO_4$ is oxidized to PbO_2. When calcium is introduced into lead-tin alloys, their electrochemical activity increases (Fig. 3).

Table 1 presents the results of our corrosion studies on the lead alloys under examination as the weight loss of electrodes as a function of the exposure time in potentiostatic conditions.

One can see (Table 1) that the binary Pb–Sn alloys with the tin content 1.5 and 2.0% possess the highest corrosion resistance. Increasing the tin content in the alloy up to 3% has resulted in significant deterioration of its corrosion properties.

An increase in the calcium content in the Pb–Sn–Ca–Al alloys leads to increased corrosion losses, especially during longer periods of corrosion. Silver and barium dopation of these alloys enhances the corrosion stability of lead–tin–calcium alloys.

The corrosion behavior of alloys is determined by their phase composition and structure.

The results of our microstructural analysis (Fig. 4) show that the alloys with 1.0 wt.% tin (b) feature coarse grains and form a regular uniform structure. Raised tin contents lead to smaller grains (c and d). This may result in that the type of corrosion may vary from formation of a continuous uniform corrosion layer to much more selective corrosion through grain borders. According to the phase diagram of Pb–Sn, with the Sn contents being 1.0, 1.5, and 2.0 wt.%, a solid solution is formed in the system [20]. On increasing the tin content up to 3.0 wt.% (e), the alloy becomes a heterophase system and has a disordered microstructure with minimum grain sizes. Corrosion becomes more regular, and its rate rises.

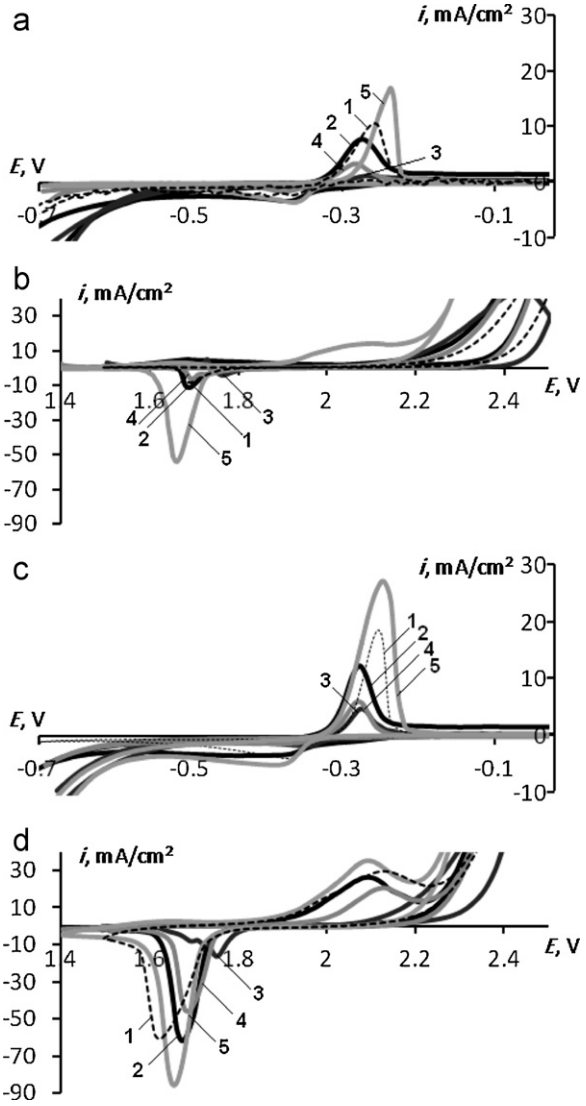

Fig. 2. Cyclic voltammogram for a Pb (1), Pb–1.0 wt.% Sn (2), Pb–1.5 wt.% Sn (3), Pb–2.0 wt.% Sn (4), Pb–3.0 wt.% Sn (5) electrodes in potential area from −0.7 to 0 V (a and c) and from 1.5 to 2.5 V (b and d) (vs. SHE). Cycle number – 1 (a and b) and 40 (c and d); scan rate – 20 mV s^{-1}.

According to the phase diagram of Pb–Sn–Ca [21], at low tin contents, calcium first quickly precipitates as Pb_3Ca like in binary lead–calcium alloys. These alloys have a fine-grain structure. Increasing the tin content switches the mode of precipitation and strengthening in time: from discontinuous Pb_3Ca precipitation to mixed discontinuous–continuous Pb_3Ca and $(PbSn)_3Ca$ precipitations, and, finally, to continuous Sn_3Ca precipitation. A lead–tin–calcium alloy with the tin content 1–1.5 wt.% contains a solid solution and fine crystals $(PbSn)_3Ca \rightarrow Sn_3Ca$. As is seen from Fig. 4, increased calcium contents result in finer grains. The 1.0 wt.% Sn, 0.08 wt.% Ca, 0.015 wt.% Al alloy has a cellular dendritic structure. Corrosion becomes more regular and preferably proceeds on interdendrite borders.

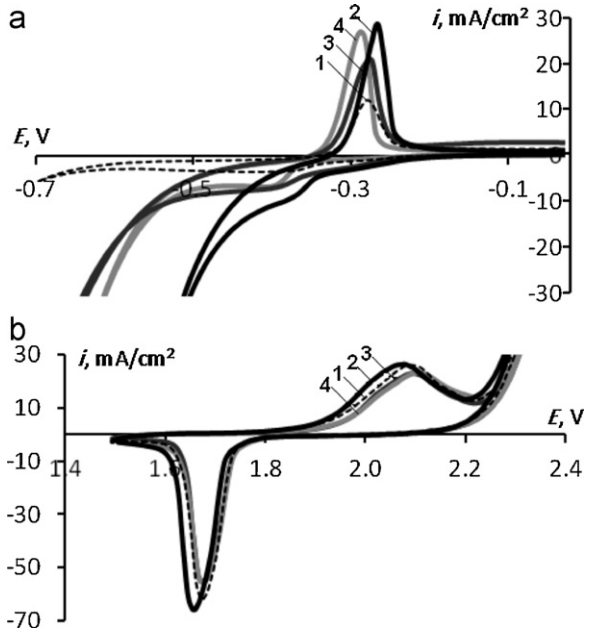

Fig. 3. Cyclic voltammogram for a Pb–1.0 wt.% Sn (1), Pb–1.0 wt.% Sn–0.01 wt.% Ca (2), Pb–1.0 wt.% Sn–0.06 wt.% Ca (3) and Pb–1.0 wt.% Sn–0.08 wt.% Ca (4) electrodes in potential area from −0.7 to 0 V (a) and from 1.5 to 2.5 V (b) (vs. SHE). Cycle number – 40; scan rate – 20 mV s^{-1}.

3.2. EIS study

On the basis of our knowledge of the processes proceeding on the lead electrode, potentials to form the corrosion layer on lead were chosen. The potential value −0.3 V corresponds to lead oxidation to lead sulfate. To explore the corrosion layer formed in a wide range of the passive state, the potential of 1.3 V was chosen within the range of deep discharge. At 1.7 V, where non-stoichiometric lead oxides are formed, $PbSO_4$ starts to oxidize to PbO_2. The 2.05 V potential is within the range where the film is mainly composed of lead (IV) oxide, this corresponds to the recharged state of the battery. There, PbO_2 is formed with no water decomposition to oxygen.

Table 1
Corrosion behavior of our alloys (E = 2.15 V, T = 40 °C, 4.8 M H_2SO_4).

Pb (wt.%)	Sn (wt.%)	Ca (wt.%)	Ag (wt.%)	Ba (wt.%)	Al (wt.%)	Weight loss ($\Delta m/S$, mg cm^{-2})			
						Polarization period, min			
						10	30	60	180
100	–	–	–	–	–	0.23 ± 0.03	0.43 ± 0.02	0.60 ± 0.06	1.0 ± 0.07
99	1.0	–	–	–	–	0.52 ± 0.01	0.57 ± 0.01	0.82 ± 0.09	1.10 ± 0.10
98.5	1.5	–	–	–	–	0.27 ± 0.02	0.34 ± 0.05	0.51 ± 0.06	1.00 ± 0.10
98	2.0	–	–	–	–	0.34 ± 0.03	0.39 ± 0.02	0.46 ± 0.03	0.91 ± 0.02
97	3.0	–	–	–	–	0.50 ± 0.03	0.57 ± 0.03	1.14 ± 0.03	1.81 ± 0.08
98.775	1.2	0.01	–	–	0.015	0.19 ± 0.03	0.38 ± 0.03	0.48 ± 0.03	1.00 ± 0.04
98.945	1.0	0.04	–	–	0.015	0.28 ± 0.02	0.56 ± 0.10	0.67 ± 0.03	1.50 ± 0.20
98.905	1.0	0.08	–	–	0.015	0.48 ± 0.01	0.61 ± 0.01	1.00 ± 0.06	2.65 ± 0.05
98.702	1.2	0.06	0.023	–	0.015	0.48 ± 0.02	0.70 ± 0.16	0.86 ± 0.06	1.19 ± 0.01
98.71	1.2	0.06	–	0.015	0.015	0.25 ± 0.02	0.36 ± 0.03	0.42 ± 0.08	1.10 ± 0.15

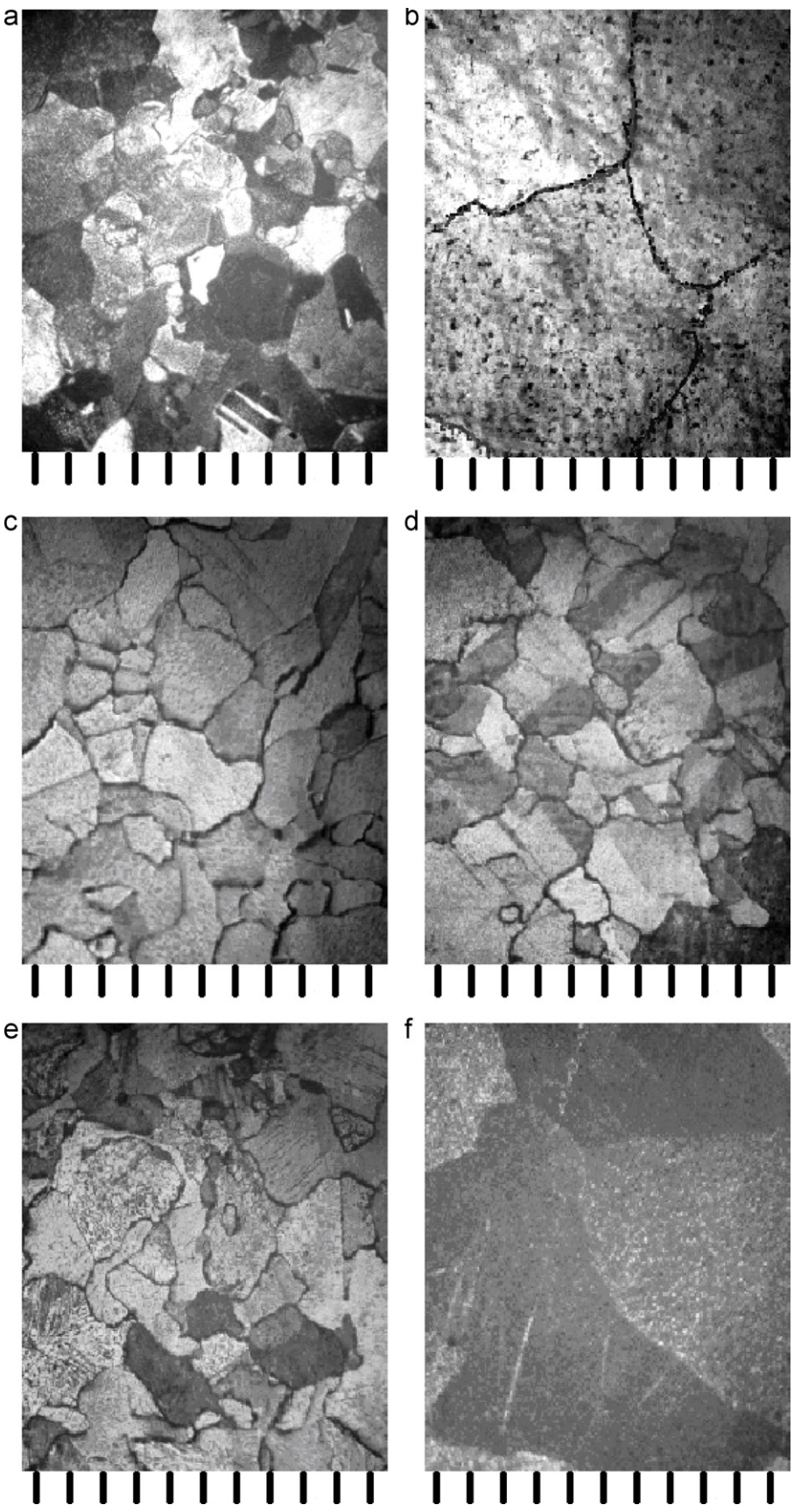

Fig. 4. Microstructure of our lead–tin alloys: (a) lead, (b) (1.0 wt.% Sn); (c) (1.5 wt.% Sn), (d) (2.0 wt.% Sn), (e) 4 (3.0 wt.% Sn), (f) (1.25 wt.% Sn, 0.01 wt.% Ca, 0.015 wt.%Al), (g) (1.0 wt.% Sn, 0.04 wt.% Ca, 0.015 wt.% Al), (h) (1.0 wt.% Sn, 0.06 wt.% Ca, 0.015 wt.%Al), and (i) (1.0 wt.% Sn, 0.08 wt.% Ca, 0.015 wt.%Al). Scale 100× (1 scale division is 0.1 mm).

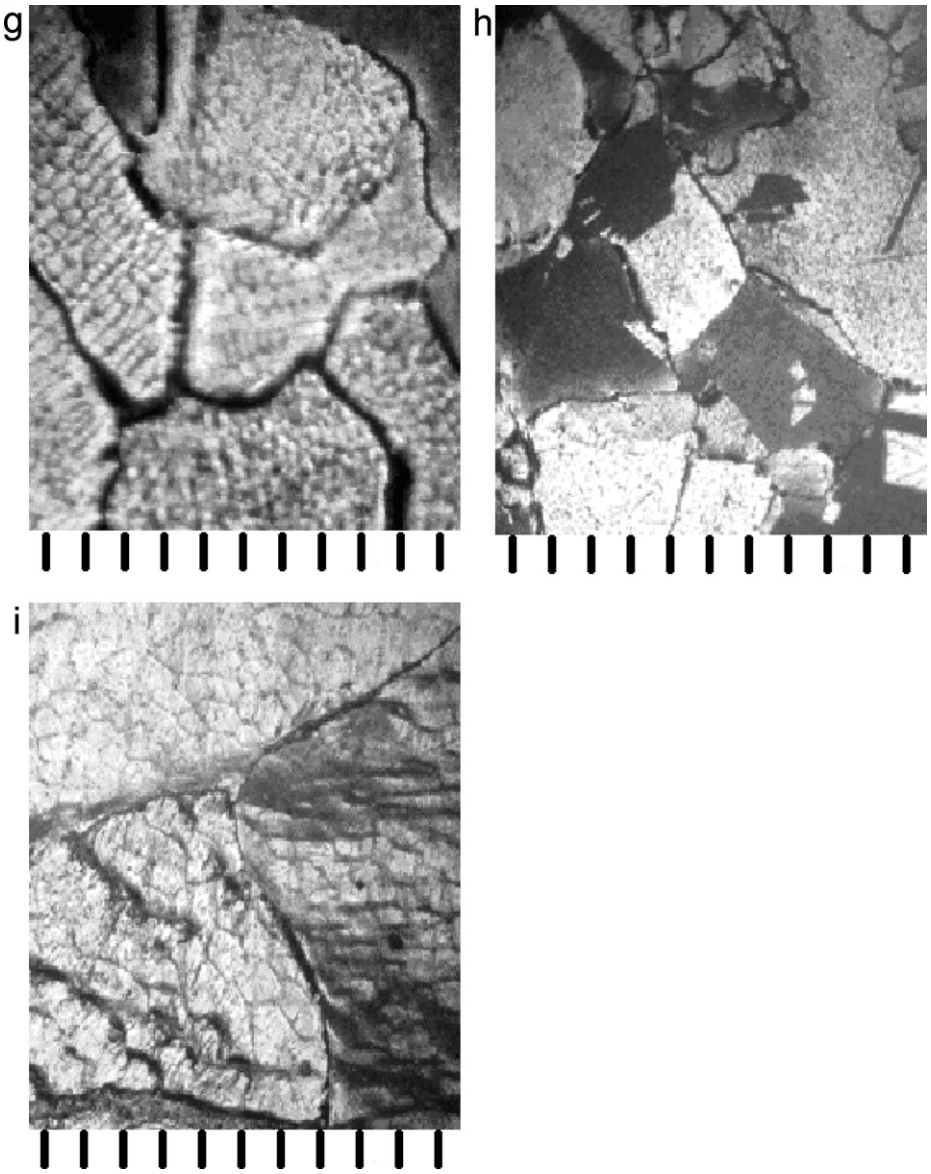

Fig. 4. (*continued*)

The scheme of growth of the corrosion film at deep discharge can be presented as follows. The positively charged surface of the lead electrode adsorbs negative sulfate ions to subsequently form a layer of lead sulfate. The formed layer of lead sulfate is a semipermeable membrane which further blocks the access of sulfate ions to the electrode surface with free movement of hydrogen ions towards any direction. This provides conditions to form α-PbO which determined a high resistance of the corrosion layer in the whole. Therefore, the corrosion film under such potentials can be presented as the double system Pb|PbO|$PbSO_4$.

Fig. 5 shows curves of the imaginary component of the impedance as a function of the real one (Nyquist plots) for the lead electrode with a corrosion film on its surface formed at several potentials — 0.3, 1.3, and 1.7 V. They look as deformed semicirclies with their center shifted under the abscissa axis The total impedance of the system can be estimated by cross section on the axis of the real part of the spectrum. It is equal to ~2.8 kΩ cm^2 for the corrosion film formed under −0.3 V while under 1.3 V the total resistance of the system is ≈150 kΩ cm^2, which is much higher than in the case of films formed at the other potentials used. Under 1.7 V, the total impedance of the system can be estimated as 65 kΩ cm^2.

The obtained frequency dependence of the electrode impedance within 0.01–50,000 Hz is best fitted by the following equivalent circuit (Fig. 6).

A similar equivalent circuit was used to describe the impedance behavior of the Pb–Ca–Sn and Pb–Ca–Sn–Li electrodes in 4.5 M H_2SO_4 at open-circuit potential (OCP) [22].

The equivalent circuit consists of the resistor R_s, capacitor C connected in parallel with the resistor R_1 and block *CPE*–R_2. The resistor R_s corresponds to the ohmic resistance of the electrolyte. The element C can be attributed to the capacity of the double electrical layer at the electrode/electrolyte ($PbSO_4$/electrolyte) interphase.

In this condition, a lead sulfate film is formed at the electrode surface, which promotes formation of a layer of lead (II) oxide under the $PbSO_4$ layer. Hence, the elements R_1 and R_2 can be correlated with the resistances of $PbSO_4$ and PbO, respectively, i.e. with the outer and inner parts of the corrosion layer.

The element CPE (constant phase element) is associated with the PbO/$PbSO_4$ interphase inside the corrosion layer. The element *CPE* characterizes the non-uniform charge distribution at the PbO/$PbSO_4$ interface, which confirms the spongy and porous structure of the lead sulfate formed. The usage of a constant phase

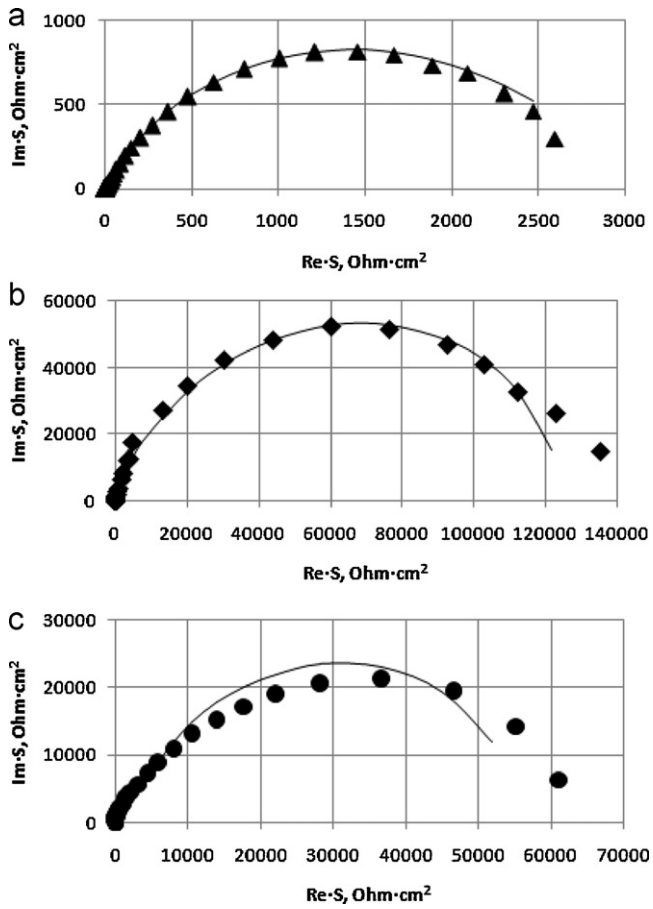

Fig. 5. The Nyquist plots for Pb electrodes with corrosion films formed on the their surface during 1 h at $E = -0.3$ (a), 1.3 (b) and 1.7 V (c) with preliminary cycling of the electrodes (5 cycles) within the range from −1.0 V to the potential of growth Experimental data (●) and fit line (–).

element allows describing the deformed nature of the semicircles on our Nyquist plots.

CPE means a constant phase element, its impedance is:

$$Z_{(CPE)} = (Y(j\omega)^n)^{-1}$$

where Y is determined by some combination of properties of both surface and electroactive part. The exponent n lies within from −1 to 1, $n = 1$ corresponds to a capacitor; $n = 0.5$ describes diffusion; and $n = 0$ implies a resistor.

The calculated values of the elements of the proposed equivalent circuit are shown in Table 2.

The resistance R_1 treated as the resistance of the external sulfate film takes on low values, which is due to the lower resistance of lead sulfate in comparison with lead oxide (10^8 and 10^{12}–10^{14} Ω, respectively) [23]. Besides, because of the porous structure, the electrolyte easily penetrates through it.

However, it should be noted that R_1 for the corrosion film obtained under 1.3 V has a higher value than those at other potentials while the capacity C has, on the contrary, a lower one. This is due to that the most dense sulfate film is formed in these conditions.

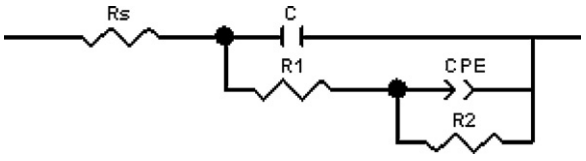

Fig. 6. Equivalent circuits for modeling of impedance data for lead electrodes with corrosion films formed at potentials (V): $E = -0.3$, 1.3, 1.7.

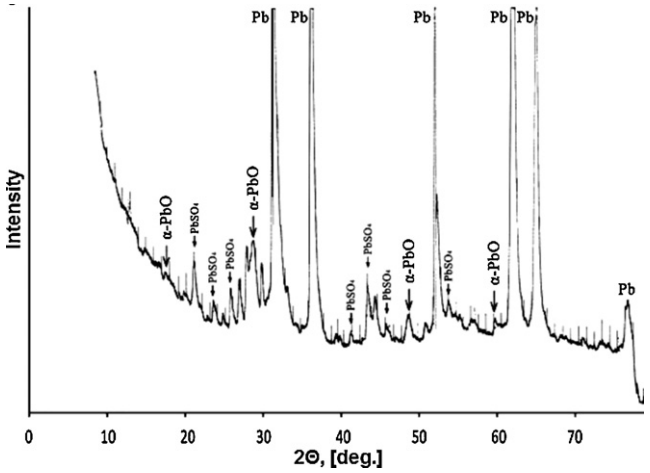

Fig. 7. X-ray analysis of lead electrode covered with a corrosion film formed during 6 h at $E = 1.3$V.

The resistance R_2 associated with the internal PbO layer has high values, and the highest ones are characteristic of the corrosion film formed under 1.3 V. These conditions correspond to a deeply discharged state of the battery, and the growth of the insulating corrosion layer quickly raises the internal resistance of the battery.

The presence of lead (II) oxide was confirmed by X-ray analysis. At least, two distinct peaks are observed on the diffraction pattern of the lead electrode with the corrosion layer formed at 1.3 V, this means the presence of α-PbO in the film (Fig. 7).

At the more positive potential 1.7 V, PbO converts into oxides with higher oxidation degrees PbO_x, which reduces the resistance of the internal oxide layer. This potential range is characterized by the onset of lead (IV) oxide formation; this substance forms a mixed phase with lead monoxide, which has a lower resistance.

The critical value of the stoichiometric coefficient x in PbO_x is approx. 1.5. Below this value, growth of the oxidation degree results in a slight rise in conductivity due to higher defect degrees of the crystal lattice of PbO when saturating with oxygen. At $x \approx 1.5$, the crystal lattice of PbO converts into PbO_2 with a relatively high electronic conductivity.

To study the influence of the duration of formation of the contact corrosion layer on its properties, lead electrodes were subjected to polarization of various durations under 1.3 V. Then, their impedance spectra were recorded and the parameters of equivalent circuits were calculated. Fig. 8 demonstrates the Nyquist curves for the films grown during 5, 30, 60, and 360 min. The equivalent circuit's parameters are given in Table 3. By estimating both the total impedance of the system and the calculated values of the circuit's

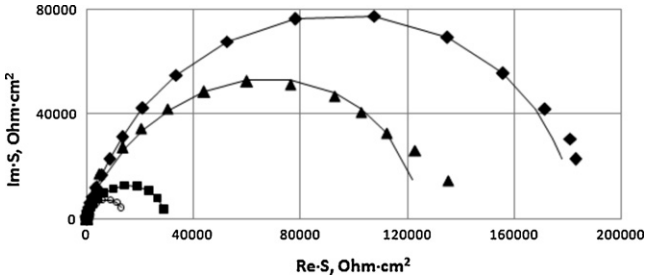

Fig. 8. Nyquist plots for lead electrodes with a corrosion film on their surface formed during 5 (○), 30 (■), 60 (▲) and 360 (♦) at potential $E = 1.3$V. Experimental data (○), (■), (▲), (♦) and fit line (–).

Table 2
Equivalent circuit parameters for lead electrodes covered with a corrosion film formed during 1 h at several potentials.

Circuit element	Potential of corrosion layer growth (V)					
	−0.3		1.3		1.7	
	Value	Fit. er. (%)	Value	Fit. er. (%)	Value	Fit. er. (%)
R_s (Ω cm^2)	0.6	3.0	0.7	10.0	0.9	4.0
C (F)	1.7×10^{-5}	3.2	2.3×10^{-6}	6.3	1.6×10^{-5}	6.4
R_1 (Ω cm^2)	3.9	5.6	12.8	6.6	4.2	14.6
CPE (Y,Ω^{-1} cm^{-2} s^n)	1.1×10^{-3}	1.8	7.4×10^{-6}	2.6	1.7×10^{-4}	1.1
CPE (n)	0.7	0.7	0.8	1.3	0.8	0.4
R_2 (Ω cm^2)	2907	2.8	133,020	2.2	55,091	2.0

Table 3
Equivalent circuit parameters for lead electrodes covered with corrosion film formed at E = 1.3 V with different polarization time, min: 5, 30, 60, 360.

Circuit element	t (min)							
	5		30		60		360	
	Value	Fit. er. (%)	Value	Fit. er. (%)	Value	Fit. er. (%)	Value	Fit. er. (%)
R_s (Ω cm^2)	0.5	4.6	0.8	6.5	0.7	10.0	0.6	11.6
C ($\times 10^6$ F)	2.6	4.6	3.8	6.7	2.3	6.3	0.3	6.2
R_1, (Ω cm^2)	2.2	7.9	10.5	12.	12.8	6.6	27.9	3.0
CPE (Y,Ω^{-1} cm^{-2} s^n)	1.4	1.6	2.2	2.2	0.7	2.5	1.0	1.6
CPE (n)	0.8	1.1	0.7	1.6	0.8	1.3	0.9	0.4
R_2 (Ω cm^2)	14,448	0.9	29,157	2.0	133,020	2.2	191,420	1.9

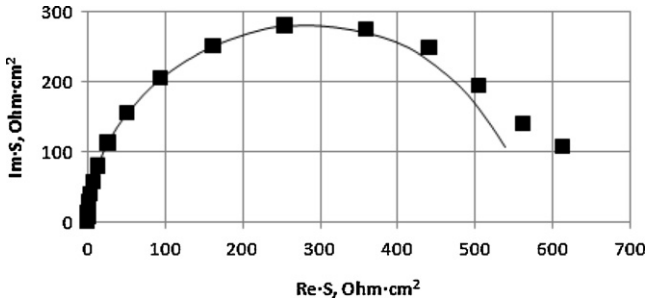

Fig. 9. Nyquist plots for lead electrode with a corrosion film on its surface formed at potential E = 2.05 V during 1 h. Experimental data (■) and fit line (–).

elements, one can see that the resistance (and, hence, thickness) of the corrosion layer increases with polarization time.

Fig. 9 shows the frequency dependence recorded for the anode film at 2.05 V. It looks as a regular circle without deformations. The polarization resistance, estimated by the cut of the semicicrle with the real part of the impedance spectrum, has the lowest value among all the potentials used (≈0.7 kΩ cm^2), which is conformed by the calculated parameters of the equivalent circuit, see Table 4. The circuit ilself comprises one block C–R connected in parallel to the Ohmic resistance R_s of the electrolyte (Fig. 10). All this means that the film formed under this potential is unilayered, compact and made of well-conducting PbO_2 with a specific resistance of 9×10^{-5} Ω m [23].

As the corrosion layer at 1.3 V possesses the worst conductivity and so can affect the performance of the battery, a study was made of the influence of most used dopants to the alloys for the positive

Table 4
Equivalent circuit parameters for lead electrodes covered with a corrosion film formed at E = 2.05 V during 1 h with pre-cycling.

Circuit element	Value	Fit. er. (%)
R_s (Ω cm^2)	0.42	1.95
C (F)	2.08×10^{-3}	1.34
R (Ω cm^2)	569.40	2.70

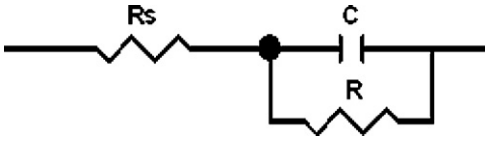

Fig. 10. The equivalent circuit for modeling of impedance data for lead electrodes with corrosion films formed at E = 2.05 V.

grids of lead-acid batteries, namely, tin and calcium, silver, barium, antinomy, and cadmium.

To study the influence of tin and calcium dopation on the properties of the corrosion film formed on the positive grid surface, electrodes made of two alloys were used, namely the lead–tin (Pb–x wt.% Sn, x = 1.0, 1.5, 2.0, 3.0) and lead–tin–calcium (Pb–1 wt.% Sn–0.08 wt.% Ca–0.015 wt.% Al). Impedance spectra were recorded in similar conditions.

Fig. 11 illustrates the Nyquist curves for the corrosion layers on pure lead and on the Pb–Sn and Pb–Sn–Ca–Al alloys. To process the data obtained, the equivalent circuit earlier proposed for the film on pure lead at 1.3 V was used. It is seen from the hodographs and calculated parameters of the circuit (Table 5) that introduction of a tin additive (1%) to lead promotes the formation of a better

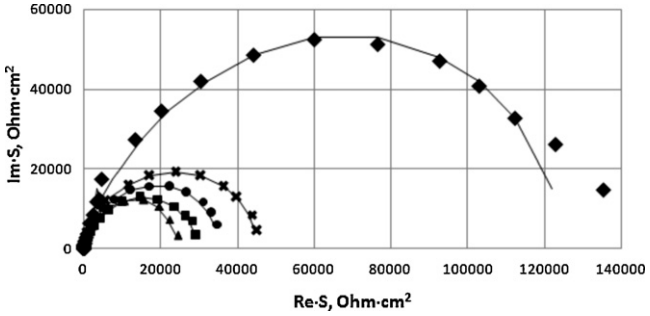

Fig. 11. Nyquist plots for Pb (♦), Pb–1.0 wt.% Sn (●), Pb–2.0 wt.% Sn (■), Pb–3.0 wt.% Sn (▲), Pb–1.0 wt.% Sn–0.08 wt.% Ca (×) electrodes with a corrosion film on their surface formed at potential E = 1.3 V during 1 h with pre-cycling. Experimental data (♦), (●), (■), (▲), (×) and fit line (–).

Table 5
Equivalent circuit parameters for the Pb, Pb–1.0% Sn, Pb–2.0% Sn, Pb–3.0% Sn, Pb–1.0% Sn–0.08% Ca–0.015 wt.% Al electrodes covered with a corrosion film formed during 1 h at E = 1.3 V with pre-cycling.

Circuit element	Pb		Pb–1.0 wt.% Sn		Pb–2.0 wt.% Sn		Pb–3.0 wt.% Sn		Pb–1.0% Sn–0.08% Ca–0.015 wt.% Al	
	Value	Fit er. (%)	Value	Fit er. (%)	Value	Fit er. (%)	Value	Fit er. (%)	Value	Fit er. (%)
R_s (Ω cm^2)	0.7	10	0.6	4.	0.7	22	0.7	5.4	0.5	4.0
C (F)	2.3×10^{-6}	6.3	2.9×10^{-6}	1.5	2.0×10^{-6}	2.5	2.3×10^{-6}	1.9	8.9×10^{-6}	3.7
R_1 (Ω cm^2)	12.8	6.6	9.1	6.0	19.1	1.6	17.8	10.5	10.4	6.7
CPE (Y,Ω^{-1} cm^{-2} s^n)	0.7×10^{-5}	2.6	1.1×10^{-5}	2.0	1.1×10^{-5}	3.1	0.9×10^{-5}	5.4	1.3×10^{-5}	3.0
CPE (n)	0.8	1.3	0.8	0.6	0.8	3.5	0.8	1.5	0.8	1.3
R_2 (Ω cm^2)	133,020	2.2	38,962	1.5	34,314	2.4	28,091	3.7	45,004	1.4

Table 6
Equivalent circuit parameters for Pb–1.2 Sn–0.06 Ca–0.015 Al–0.015 Ba, Pb–1.25 Sn–0.06 Ca–0.015 Al–0.023 Ag electrodes covered with a corrosion film formed during 1 h at E = 1.3 V with pre-cycling.

Alloy	Pb–1.0Sn–0.08Ca–0.015Al		Pb–1.2Sn–0.06Ca–0.015Al–0.015Ba		Pb–1.25Sn–0.06Ca–0.015Al–0.023Ag	
Circuit element	Value	Fit. Er. (%)	Value	Fit. Er. (%)	Value	Fit. Er. (%)
R_s (Ω cm^2)	0.5	4.0	0.6	7.6	1.4	22.0
C (F)	8.9×10^{-6}	3.7	2.0×10^{-6}	1.2	7.3×10^{-7}	3.0
R_1 (Ω cm^2)	10.4	6.7	24.2	13.0	85.0	13.1
CPE (Y,Ω^{-1} cm^{-2} s^n)	1.3×10^{-5}	3.0	5.5×10^{-6}	2.6	5.8×10^{-6}	3.9
CPE (n)	0.8	1.3	0.8	0.9	0.8	0.9
R_2 (Ω cm^2)	45,004	1.3	34,246	1.2	53,864	2.7

conducting corrosion layer. The resistance responsible for the oxide part of the film reduces significantly (approx. by 90 kΩ cm^2), while the resistance of sulfate remains almost the same, decreasing by 1–2 kΩ cm^2.

When the tin content in the Pb–Sn alloys is increased, this trend remains.

The conductivity of the corrosion layer formed on the Pb–Sn–Ca–Al electrode is somewhat worse than that for the Pb–Sn one.

One can conclude that tin dopation promotes the formation of a more conducting oxide layer.

X-ray phase analysis of the electrodes made of the lead–tin and lead–tin–calcium–aluminum alloys with a corrosion film on their surface formed at E = 1.3 V during 6 h has shown traces of PbO and SnO_2 in the samples.

Therefore, tin addition strongly decreases the thickness of the α-PbO layer. This may be caused by that the intergrain borders enriched with tin provide a high tin level in the corrosion layer, which may have suppressed passivation. Similar conclusions are made in [24].

Enough of tin changes alloy crystallization conditions, and significantly decreases $PbSO_4$ and α-PbO formation.

Finally, the passive layer getting thinner may be explained by the acidic nature of Sn^{4+}, which is inconsistent with the stability of α-PbO.

Tin can reduces PbO to lead, oxidizing itself to SnO_2. This decreases the pH in the near-electrode layer and, hence, prevents further influence of the alkaline medium and formation of PbO and basic lead oxides.

The increased conductivity of the corrosion layer can be also explained by the semiconductor structure of PbO doped with SnO_2.

Calcium, as an active metal, can alkalinize the near-electrode layer and promote the formation of lead (II) oxide layers, which can explain the slight worsening of the corrosion layer conductivity on the Pb–Sn–Ca–Al alloys in comparison with the Pb–Sn one.

It has been supposed [25] that in lead–calcium grids, the calcium presented on the corroded surface grid|AM as Pb_3Ca or CaO may have contribution to the increased alkalinity in the layer.

The surface morphology of the passive film formed on electrodes made of lead and the alloys under study was explored by means of scanning electron microscopy. The photos obtained are shown in Fig. 12. As is clear from Fig. 12 a fine crystalline film is formed on the surface of the lead electrode while the tin-doped alloy exhibits coarse crystals of prismatic shape, which may result in an enhanced porosity of the film.

The influence of barium and silver additives on the corrosion layer conductivity is demonstrated in Fig. 13 and Table 6. As can be seen from the data obtained, barium introduction into the lead–calcium–tin alloy decreases the resistance of the internal oxide part of the corrosion layer, while a silver additive leads to an increase of the resistance of both sulfate and oxide parts of the corrosion film.

As is known, reduction of the antimony content in lead–antimony alloys decreases the conductivity of the corrosion layer. Hence, low-antimony alloys have to be doped with additional components. Cadmium can be such a dopant. As Fig. 14 and Table 7 show, cadmium introduction into a low-antimony

Table 7
Equivalent circuit parameters for Pb–4.9 Sb–0.24 Sn, Pb–1.9 Sb–0.2 Sn, Pb–1.5 Sb–1.5 Cd electrodes covered with a corrosion film formed during 1 h at E = 1.3 V with pre-cycling.

Alloy	Pb–4.9Sb–0.24Sn		Pb–1.9Sb–0.2Sn		Pb–1.5Sb–1.5Cd	
Circuit element	Value	Fit. Er. (%)	Value	Fit. Er. (%)	Value	Fit. Er. (%)
R_s (Ω cm^2)	0.8	11.8	1.2	7.7	0.6	15.5
C (Φ)	8.3×10^{-7}	1.1	2.6×10^{-6}	4.7	1.2×10^{-6}	1.5
R_1 (Ω cm^2)	72.5	7.1	29.7	–	22.3	–
CPE (Y,Ω^{-1} cm^{-2} s^n)	5.9×10^{-6}	1.2	6.2×10^{-6}	3.3	5.2×10^{-6}	2.6
CPE (n)	0.8	0.3	0.8	1.3	0.7	1.0
R_2 (Ω cm^2)	58,028	0.8	80,441	1.8	65,867	1.6

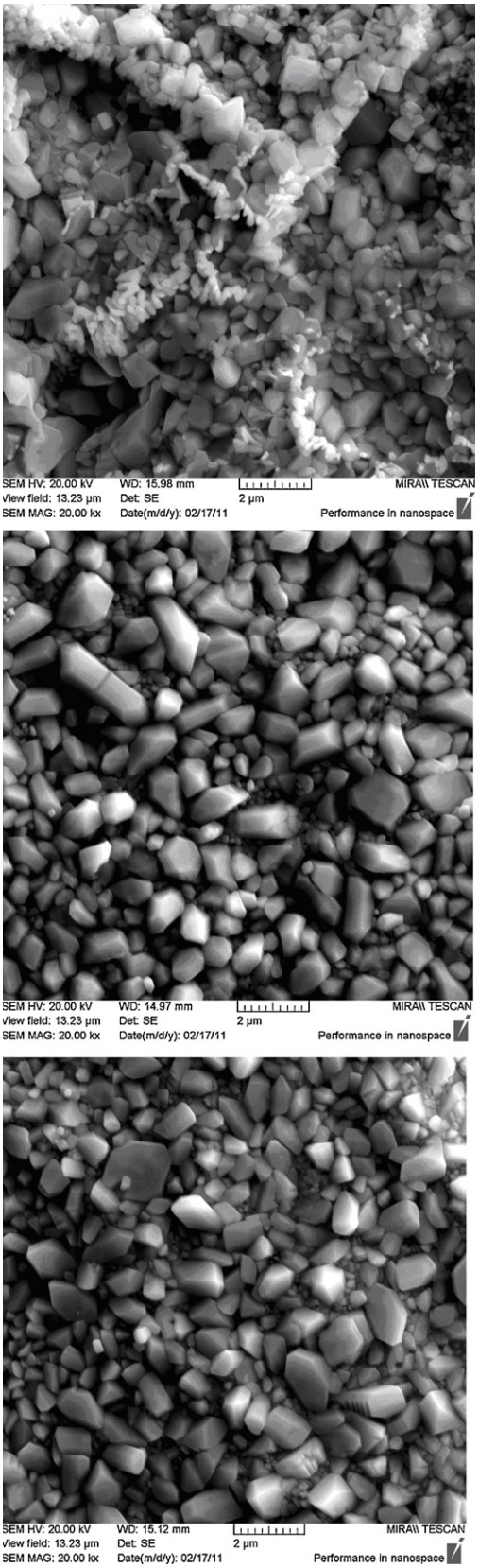

Fig. 12. SEM images of the corrosion layer on the Pb, Pb–1.0 Sn, Pb–1.0 Sn–0.08 Ca alloy electrodes.

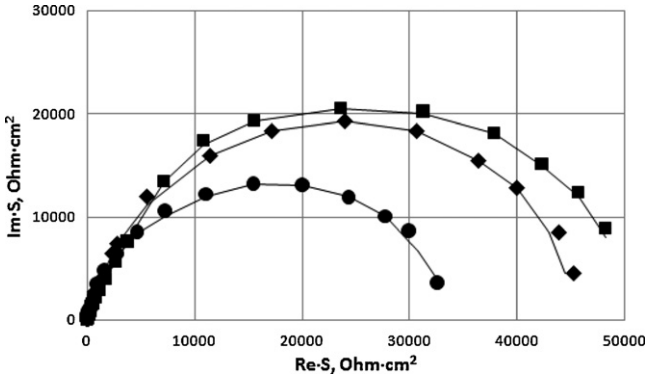

Fig. 13. Nyquist plots for several Pb–1.0 wt.% Sn–0.08 wt.% Ca–0.015 wt.% Al (⧫), Pb–1.2 wt.%Sn–0.06 wt.% Ca–0.015 wt.% Al–0.015 wt.% Ba (●), and Pb–1.25 wt.% Sn–0.06 wt.% Ca–0.015 wt.% Al–0.023 wt.% Ag (■) alloys electrodes with a corrosion film on their surface formed at potential $E = 1.3$ V during 1 h with pre-cycling. Experimental data (⧫), (●), (■) and fit line (–).

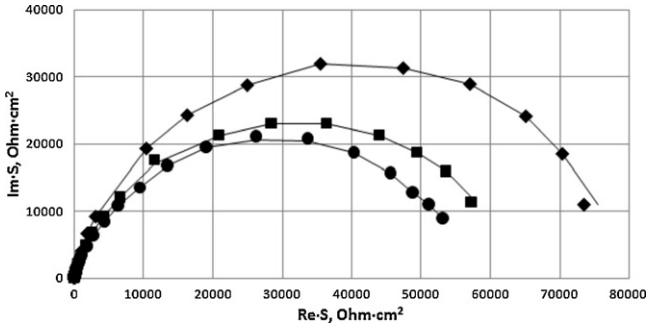

Fig. 14. Nyquist plots for Pb–4.9 wt.% Sb–0.24 wt.% Sn (●), Pb–1.9 wt.% Sb–0.2 wt.% Sn (⧫) and Pb–1.5 wt.% Sb–1.5 wt.% Cd (■) alloys electrodes with a corrosion film on their surface formed at potential $E = 1.3$ V during 1 h with pre-cycling. Experimental data (⧫), (●), (■) and fit line (–).

alloy reduces the corrosion layer resistance, and its value gets close to that for a high-antimony alloy.

4. Conclusions

1. The study of the electrochemical behavior of lead–tin and lead–tin–calcium alloys in 4.8 M sulfuric acid by means of cyclic voltammetry has shown that an increase the tin content in the lead–tin alloys from 1.0 up to 2.0 wt.% results in a decrease of the electrochemical activity of the electrodes made of these alloys in comparison with pure lead. Further increasing the tin concentration in the alloy up to 3% significantly raises its electrochemical activity within both the Pb oxidizes to $PbSO_4$ and $PbSO_4$ oxidizes to PbO_2. When calcium is introduced into the lead–tin alloys, their electrochemical activity enhances in the potential range from −0.7 to 0.0 V. In the range of high anode potentials, calcium introduction almost does not affect the oxidation rate of lead sulfate to lead dioxide.
2. The corrosion stability of lead–tin and lead–tin–calcium alloys in sulfuric acid solution was examined. The binary Pb–Sn alloys with tin contents of 1.5 and 2.0% have been found to possess the best corrosion stability. Increasing the tin content in the alloy up to 3% resulted in a significant decrease of its corrosion resistance. Higher calcium contents in the Pb–Sn–Ca alloys lead to higher corrosion losses, especially at long corrosion exposures. Dopation of these alloys with silver and barium enhances their corrosion stability.
3. The results of our electrochemical and corrosion studies agree well with the data of micro-structural analysis of the alloys.

The lead–tin alloys with tin concentrations below 2.0 wt.% have been established to have a regular uniform structure, and higher tin contents result in smaller grains. During this, the corrosion type switches from the formation of a continuous corrosion layer to selective corrosion along the grain borders. The lead–tin alloy with 3.0 wt.% of tin is a heterophase system and has a disordered microstructure with the smallest grains, which promotes its corrosion.

Lead–tin–calcium alloys have a coarse-grain structure. Increasing the calcium content in such an alloy results in smaller grains and larger intercrystallite zones; their corrosion gets more regular and preferably occurs on the intercrystallite borders. This increases the corrosion rate of the lead–tin–calcium alloys with high calcium percentages.

4. The X-ray analysis has found the passivating film formed at oxidation of the lead electrode at 1.3 V (the range of deep discharge) contains lead oxide (II) as well as lead sulfate. Therefore, the corrosion film in these conditions can be considered as a two-layered one: $Pb|PbO|PbSO_4$.
5. The properties of the corrosion layers formed on the surface of the lead electrode under potentials corresponding to various discharge degrees of the working electrodes of the lead-acid battery were studied by means of impedance spectroscopy. At potentials of −0.3, 1.3, and 1.7 V in 4.8 M sulfuric acid, the electrode impedance of the lead electrode can be represented by an equivalent circuit, which provides the formation of a two-layered film (lead sulfate and oxide (II)) on the electrode surface. The maximum resistance of the corrosion layer was observed at a potential 1.3 V (vs. SHE) within the deep battery discharge range. Lead oxide (II) under the lead sulfate layer is responsible for the high resistance of the contact corrosion layer on the lead electrode. The corrosion film formed at 2.05 V is single-layered, compact, and composed of well-conducting PbO_2. The calculated parameters of our proposed equivalent circuits confirm this conclusion.
6. Tin addition to lead reduces the corrosion layer resistance due to thinning of the lead oxide's part of the passivating film. Calcium introduction into the lead–tin alloy raises the impedance of the system insignificantly.
7. The surface morphology of pure lead, lead–tin and lead–calcium–tin alloys was analyzed by means of SEM. A fine-crysytalline film is formed on the surface of the lead elecftrode while tin-doped lead shows large prismatic crystals, that might increase the porosity of the sulfate film.
8. Barium dopation of lead–calcium–tin alloy results in an increased conductivity of the corrosion layer, while a silver additive somewhat raises the total impedance of the system.
9. For low-antimony lead alloys, cadmium addition with an equimolar ratio relative to antimony promotes increasing the conductivity of the contact corrosion layer.
10. The results of our work can be useful in obtaining and testing of new multicomponent lead alloys for hermetical lead-acid batteries, and can also serve a methodical basis for designing of indestructible techniques for testing of the resistance of contact corrosion layers immediately in batteries during their operation and storage.

References

[1] D. Pavlov, J. Power Sources 53 (1995) 9.
[2] D. Pavlov, J. Electroanal. Chem. 118 (1981) 167.
[3] Y. Gou, J. Electrochem. Soc. 138 (1991) 1222.
[4] R.D. Prengaman, J. Power Sources 53 (1994) 207.
[5] G.J. May, J. Power Sources 59 (1996) 147.
[6] R.D. Prengaman, J. Power Sources 95 (2001) 224.
[7] D.W.H. Lambert, J.E. Manders, R.F. Nelson, K. Peters, D.A.J. Rand, M. Stevenson, J. Power Sources 88 (2000) 130.
[8] N. Bui, P. Simon, N. Pebere, J. Power Sources 73 (1998) 30.
[9] E. Rocca, J. Steinmets, Elektrochim. Acta 44 (1999) 4611.
[10] Yu. Kamenev, A. Kiselevich, E. Ostapenko, Yu. Skachkov, Elektrokhimicheskaya energetika 1 (2001) 17.
[11] G.W. Mao, P. Rao, J.F. Trenter, US Patent 4,166,155 (1979).
[12] D.A.J. Rand, P.T. Moseley, J. Garche, C.D. Parker (Eds.), Valve-regulated Lead-acid Batteries, Elsevier, 2004.
[13] L. Albert, A. Chabrol, L. Torcheux, Ph. Steyer, J.P. Hilger, J. Power Sources 67 (1997) 257.
[14] N. Bui, P. Mattesco, P. Simon, J. Steinmetz, E. Rocca, J. Power Sources 67 (1997) 61.
[15] P. Mattesco, N. Bui, P. Simon, L. Albert, J. Power Sources 64 (1997) 21.
[16] Yu. Kamenev, A. Kiselevich, E. Ostapenko, Yu. Skachkov, Russ. J. Appl. Chem. 75 (2002) 562.
[17] E. Rocca, G. Bourguignon, J. Steinmets, J. Power Sources 161 (2006) 666.
[18] P. Rao, US Patent 5,298,350 (1994).
[19] E. Jullian, L. Albert, J.L. Caillerie, J. Power Sources 116 (2003) 185.
[20] A.E. Wal, Structure and Properties of Double Metallic Systems, Fizmatgiz, Moscow, 1959.
[21] J. Herts, C. Fornasieri, J.P. Hilger, M. Notin, J. Power Sources 46 (1993) 299.
[22] R.K. Shervedani, A.Z. Isfahani, R. Khodavisy, A. Hatefi-Mehrjardi, J. Power Sources 164 (2007) 890.
[23] A.A.K. Vervaet, D.H.J. Baert, Electrochim. Acta 47 (2002) 3297.
[24] R. Miraglio, L. Albert, A. El Ghachcham, J. Steinmetz, J.P. Hilger, J. Power Sources 53 (1995) 53.
[25] R.D. Prengaman, Proc. 4th International Lead-Acid Battery Seminar, 25–27 April, 1990, San Francisco, CA, USA, International Lead Zinc Research Organization Inc., Research Triangle Park, NC, USA, 1990, pp. 19–30.